AGU PUBLICATIONS

JGR

Journal of Geophysical Research: Earth Surface

RESEARCH ARTICLE
10.1002/2016JF003855

Key Points:
- Ice-sheet growth and decay produce geologically rapid changes in lithospheric loading and stress
- Simulated differential stresses from loading are of a similar magnitude to those needed for dike and vug-wave magma migration processes
- Cyclic loading might aid magma ascent and eruption, enhancing subglacial geothermal heat flux

Supporting Information:
- Supporting Information S1

Correspondence to:
N. T. Stevens,
nate.t.stevens@gmail.com

Citation:
Stevens, N. T., B. R. Parizek, and R. B. Alley (2016), Enhancement of volcanism and geothermal heat flux by ice-age cycling: A stress modeling study of Greenland, *J. Geophys. Res. Earth Surf.*, *121*, doi:10.1002/2016JF003855.

Received 10 FEB 2016
Accepted 4 AUG 2016
Accepted article online 6 AUG 2016

Enhancement of volcanism and geothermal heat flux by ice-age cycling: A stress modeling study of Greenland

Nathan T. Stevens[1,2], Byron R. Parizek[3], and Richard B. Alley[1]

[1]Department of Geosciences and the Earth and Environmental Systems Institute, Pennsylvania State University, University Park, Pennsylvania, USA, [2]Department of Earth and Atmospheric Sciences, Cornell University, Ithaca, New York, USA, [3]Mathematics and Geosciences, Pennsylvania State University, DuBois, Pennsylvania, USA

Abstract Ice-age cycling of the Greenland ice sheet likely contributed to locally elevated subglacial geothermal heat fluxes (GHFs), based on recent thermal modeling. Borehole and geophysical data indicate higher GHF in some areas than suggested by current knowledge of underlying geology, particularly at the head of the Northeast Greenland Ice Stream. Changes in lithospheric loading during ice-sheet growth and decay cycles produce large and geologically rapid changes in the effective stress state beneath and near the ice sheet. Oscillations in melt fraction from cyclic loading through multiple ice-age cycles will enhance upward magma migration through the nonlinear increase of melt migration velocity with melt fraction. We simulate periodic ice-sheet loading scenarios along an east-west transect across central Greenland on an Elastic Lithosphere, Relaxed Asthenosphere Earth model. Under likely parameter ranges, deviatoric stresses in the elastic lithosphere across widespread regions are sufficiently high to meaningfully enhance dike emplacement and also allow vug-wave propagation in some scenarios. Stress patterns migrate laterally in response to ice-sheet dynamics, favoring multistage magma ascent. If melt occurs at depth, our modeling suggests that ice-age cycling could help it migrate upward to shallow depth or erupt, contributing to the high observed GHF. Furthermore, shallow magma emplacement might feed hydrothermal systems exploiting enhanced faulting or fracturing from ice-age cycling, adding to elevated GHF. The preglacial passage of the Iceland-Jan Mayen hot spot could have sourced such magmas. Direct observations of these lithospheric processes needed to further constrain our models are limited, highlighting the value of more targeted geophysical studies informing future modeling.

1. Introduction

Geothermal heat flux (GHF) is important for ice-sheet basal melting and lubrication [e.g., *Pollack et al*., 1993; *Parizek et al*., 2002, 2003; *Pollard et al*., 2005; *Cuffey and Patterson*, 2010; *Joughin et al*., 2010; *Larour et al*., 2012]. Recent geophysical investigations and coring suggest anomalously high GHF values beneath central regions of the Greenland ice sheet (GrIS) [*Pollack et al*., 1993; *Fahnestock et al*., 2001; *Dahl-Jensen et al*., 2003b]. The track of the Iceland-Jan Mayen hot spot crossed the island and may have contributed to somewhat thinner lithosphere and higher GHF than typical for an Archean craton, although it remains difficult to link modern GHF observations with the timeline of the hot spot's passage between ~90 Ma and ~30 Ma [*Müller et al*., 1993; *Braun et al*., 2007]. Figure 1a shows the envelope of several previously published hot spot tracks, which includes the region of rapid basal melting near the head of the Northeast Greenland Ice Stream [*Lawver and Müller*, 1994; *Shapiro and Ritzwoller*, 2004; *Fox-Maule et al*., 2005, 2009; *Greve*, 2005; *Braun et al*., 2007; *Petrunin et al*., 2013; *Rickers et al*., 2013].

Numerous studies have shown that pressure changes and flexural stresses associated with the glacial isostatic adjustment (GIA) caused by glacier and ice-sheet mass changes must affect the volume and migration of magma in the rocks beneath, with enhanced magma extraction during deglaciation contributing to increased eruptive frequency or volume [e.g., *Hall*, 1982; *Hardarson and Fitton*, 1991; *Sigvaldason et al*., 1992; *Zielinski et al*., 1994, 1996; *Huybers and Langmuir*, 2009; *Sternai et al*., 2016]. Furthermore, these stresses have been associated with shallow crustal fracturing and faulting, which likely increase shallow crustal permeability and porosity for groundwater flow within some glaciated settings [*Wu and Hasegawa*, 1996; *Stewart et al*., 2000; *Hampel and Hetzel*, 2006].

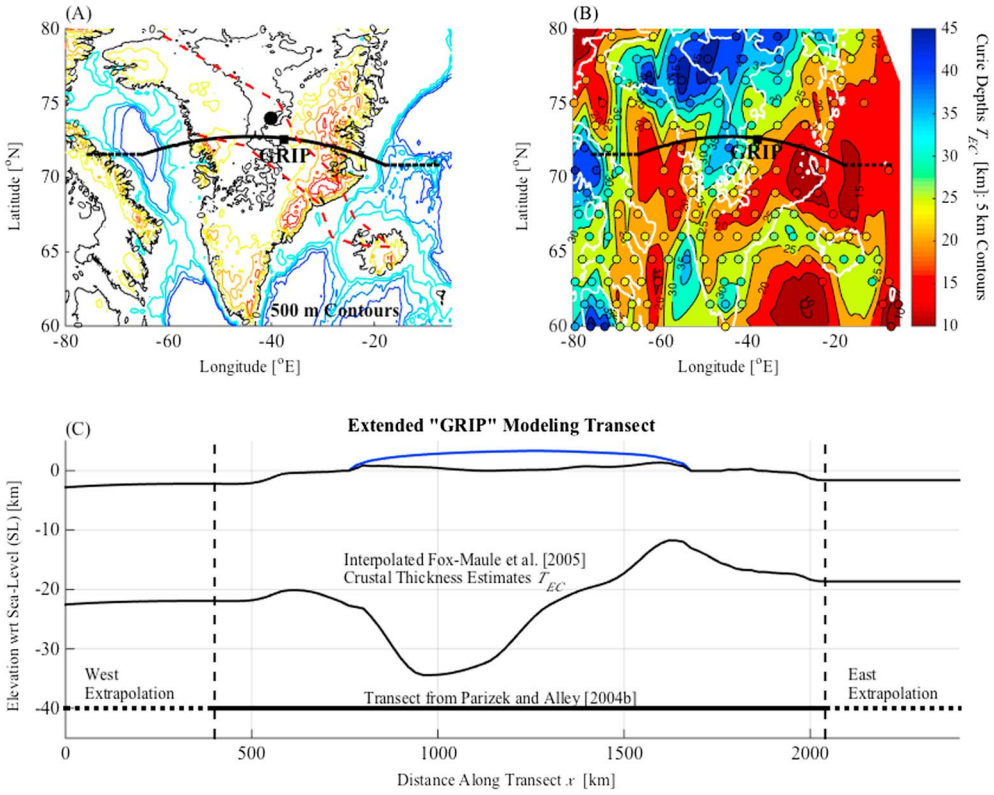

Figure 1. Modern topography, ice thickness, and elastic crustal thickness estimates along the 2400 km long extended "GRIP" transect [after *Parizek and Alley*, 2004]. (a) Transect across central Greenland (thick black line), overlain on modern bedrock topography (colored contours) with sea level (SL) in black [*Amante and Eakins*, 2009]. The zone containing estimates of the Iceland hot spot track (red dashed outline [*Braun et al*., 2007]) and the approximate location of high basal melting (large black dot [*Fahnestock et al*., 2001]) are shown for reference. Transect extrapolations (dashed black lines) are included to prevent edge effects in stress modeling. (b) Raw (colored dots) and cubically interpolated (5 km interval colored contours) Curie depth estimates (the 580°C isotherm) [after *Fox-Maule et al*., 2005]. Modern SL is shown for reference (white contour). (c) The parameterized GRIP transect, showing modern ice-surface elevation (blue line), bedrock topography (upper black line) from Figure 1a, and interpolated Curie depths (lower black line) from Figure 1b.

We hypothesize that the geologically rapid (tens to hundreds of kiloyears) changes in lithospheric stress from ice-age cycling of the GrIS enhanced magma ascent and/or fracture-hosted deep groundwater circulation, contributing to the observed GHF anomalies observed. We qualitatively summarize a possible role for oscillating load from ice-age cycling in enhancing melt extraction through percolation. We then test the plausibility of this mechanism by applying computationally efficient simulations to estimate deviatoric stress fields during glacial/interglacial cycling of the GrIS, finding widespread stresses similar to those estimated to cause dike propagation in magmatic systems. Together, these support our hypothesis that ice-sheet processes might have contributed to anomalous GHF, and we argue that more targeted geophysical studies [e.g., *Pourpoint et al*., 2015] informing higher-order modeling are required to advance this work.

1.1. Ice-Sheet Enhancement of Melt Extraction and Migration

The onset of glaciation over a partially molten, deep region of lithosphere would reduce melt production and also melt fraction there as a roughly linear function of the ice-sheet load, with deglaciation returning melt fraction either to the original value or to a somewhat higher value in regions with additional unloading associated with active glacier erosion and sediment evacuation [*Sternai et al*., 2016]. Even within regions of negligible net erosion, if ice-age cycling occurred for a sufficiently long time to lose dependence on initial conditions, then a glacial cycle with larger oscillations would extract melt more efficiently, because buoyant ascent of distributed melt increases as the square of the melt fraction above some percolation threshold [*McKenzie*, 1984; *McKenzie and Bickle*, 1988; *Connolly et al*., 2009; *Kohlstedt and Holtzman*, 2009]. Our simulations suggest the possibility that this process affected Greenland and may also have affected other glaciated

regions such as West Antarctica, potentially motivating further research. Here we focus primarily on the flexural effects of ice-age cycling on lithospheric stresses beneath GrIS.

Upward magma migration through dike propagation requires fracture-opening stresses of order 10 MPa, depending on the magma and rock types [*Rubin*, 1995a, 1995b], arising from some combination of magma pressure and horizontal deviatoric stress σ'_{xx} [*Cooper*, 1990; *Wu and Hasegawa*, 1996; *Klemann and Wolf*, 1998; *Stewart et al*., 2000]. Similarly, shear stress magnitudes $\left(\left|\tau'_{xz}\right|\right)$ of a few tenths to tens of MPa may aid magma ascent through vug-wave migration (the migration of magma in waves of small pockets, aka vugs, along shear planes within a deforming host rock), depending on system parameters [*Phipps Morgan and Holtzman*, 2005]. In what follows, we consider scenarios in which preexisting magmas at depth may be pushed past these stress thresholds by additional contributions from flexural differential stresses. Magma clearly is emplaced at some times and some places by processes completely independent of ice loading, so Earth processes clearly generate the stress magnitudes of ~10 MPa for dike emplacement [*Rubin*, 1995a, 1995b] and ~1 MPa or more for vug-wave propagation [*Phipps Morgan and Holtzman*, 2005]. Here we consider GIA stresses to be significant if they are of the same order of magnitude as these values, and we thus focus on horizontal stresses $\sigma'_{xx} \leq -3$ MPa and vertical shear stresses $|\tau'_{xz}| \geq 0.3$ MPa.

Modern ice sheets have grown and shrunk during ice-age cycles over hundreds of thousands to millions of years. Over these timescales, crust and upper mantle lithosphere likely behave elastically, likely decoupled by a ductile lower crust [*Burov and Diament*, 1992, 1995; *Kohlstedt et al*., 1995; *Klemann and Wolf*, 1998]; however, seismic observations and thermal modeling suggest that the crust provides most of the flexural strength on ice-age timescales in some settings [*Maggi et al*., 2000; *McKenzie et al*., 2005]. In the following sections, we model differential tensile and shear stresses generated by ice-age cycling in the elastic crust beneath the Greenland ice sheet along the west-east Greenland Ice Core Project (GRIP) transect of *Parizek and Alley* [2004], incrementally parameterized with modern topography, ice-sheet thickness, and elastic crustal thickness estimates shown in Figure 1 [*Letréguilly et al*., 1991; *Ekholm et al*., 1995; *Ritz and Grenoble team members*, 1997; *Maggi et al*., 2000; *Watts*, 2001; *Fox-Maule et al*., 2005; *McKenzie et al*., 2005].

2. Numerical Methods

To estimate flexure-induced differential stresses that might aid magma ascent during ice-sheet growth and decay, we conduct numerical simulations along the transect of Greenland shown in Figure 1. Building upon previous work, we simulate ice-sheet/lithosphere interactions using an adaptation of the Pennsylvania State University/University of Chicago (PSU/UofC) thermomechanical flow line model [*Parizek*, 2000, 2003; *Parizek and Alley*, 2004; *Parizek et al*., 2005]. Similar to other ice-sheet models, this finite element model implements the Elastic Lithosphere, Relaxed Asthenosphere (ELRA) treatment of isostasy coupled to a vertically integrated (1-D) Shallow Ice Approximation (SIA) of ice dynamics to estimate coupled ice flow and bedrock deflection. We first simulate stress fields in a uniform Earth model in response to ice-sheet loading, then vary elastic parameters individually to assess parameter sensitivity, and finally introduce geophysical constraints from modern lithospheric geometry beneath our transect to assess stress-field perturbations as they pertain to a Greenland-like crustal transect.

2.1. Governing Equations

The ELRA treatment approximates the surface deflection profiles of more-complex full-Earth models [e.g., *Lliboutry*, 1965; *Brotchie and Silvester*, 1969; *Le Meur and Huybrechts*, 1996], coupling the Euler-Bernoulli (thin elastic plate) bending model with a rate equation that includes a limiting time constant that emulates the deformation-retarding effect of viscous asthenospheric flow. ELRA is widely used in ice-flow modeling because of its fidelity in many cases and computational efficiency, although it may introduce errors in some cases, especially associated with steep gradients from strong ablation zones [e.g., *van den Berg et al*., 2008]. In order to build on previous work we capitalize on the strengths of ELRA in the ensemble testing of our hypothesis, we conduct simulations for a wide range of solid-Earth properties and ice loading histories in order to capture the full spectrum of plausible deflection profiles for our GrIS transect.

The EL treatment of lithospheric flexure is

$$D_{\text{lith}} \frac{\partial^4 w}{\partial x^4} = q - \rho_{\text{asth}} g w \tag{1}$$

where D_{lith} is the flexural rigidity of the lithosphere, w the deflection profile, q the downward loading force from the ice-sheet, and $\rho_{\text{asth}} g w$ the upward buoyant force from displaced asthenosphere. The RA treatment of asthenospheric flow is

$$\frac{\mathrm{d}b_r}{\mathrm{d}t} = \frac{1}{\tau_{\text{asth}}} \left(w - b_{r,o} - b_r \right) \tag{2}$$

where b_r is the bedrock profile at time t, $b_{r,o}$ the equilibrium bedrock profile in the absence of an ice load, and τ_{asth} the characteristic response time for asthenospheric flow, which is proportional to asthenospheric viscosity and inversely proportional to the wavelength of the load. Following sensitivity results from *Le Meur and Huybrechts* [1996] and *Huybrechts* [2002], we use $\tau_{\text{asth}} = 3$ kyr for all model runs. We note that selecting alternative plausible values for τ_{asth} would impact details of the transient evolution of lithospheric stresses with glacial-interglacial loading cycles (discussed further in section 3), but not the broader conclusions drawn here. The ELRA flexure model is solved using a forward Euler method.

The SIA model is fully described in *Parizek* [2000, 2003] and *Parizek et al*. [2005]. We implement results from these studies to emulate ice thickness (h_{ice}) and velocity trends, using

$$\frac{\mathrm{d}h_{\text{ice}}}{\mathrm{d}t} = \frac{\partial}{\partial x} \left(\lambda \frac{\partial s}{\partial x} \right) + \dot{A} - \dot{B} \tag{3}$$

where λ is the effective diffusivity of ice flow, s the surface elevation profile, $\dot{A}$ the ice-equivalent surface accumulation rate, and $\dot{B}$ the basal melting rate. Assuming that λ is an elemental constant in our finite element method treatment, it can be removed from within the partial differential and decomposed into the sum of sliding ($\lambda_{o,\text{slide}}$, equation (4)) and internal deformation ($\lambda_{o,\text{def}}$, equation (5)) components:

$$\lambda_{o,\text{slide}} = -h_{\text{ice}} C \left(\rho_{\text{ice}} g h_{\text{ice}} \frac{\mathrm{d}s}{\mathrm{d}x} \right)^{m-1} \rho_{\text{ice}} g h_{\text{ice}} \tag{4}$$

$$\lambda_{o,\text{def}} = \left(\frac{2}{5} \right) F_{\text{ice}} A_o (\rho_{\text{ice}} g)^{n-1} h_{\text{ice}}^{n+2} \tag{5}$$

where C is the sliding coefficient ($C = 1 \times 10^{-8}\,\text{m s}^{-1}\,\text{Pa}^{-2}$), ρ_{ice} the density of ice (910 kg/m^3), m the sliding exponent ($m = 2$), F_{ice} the ice softness enhancement factor, A_o the vertically integrated ice softness parameter, and n the flow law exponent ($n = 3$) [e.g., *Glen*, 1955; *Parizek*, 2000, 2003; *Parizek et al*., 2005]. The SIA is solved using a reverse Euler scheme, and the combined SIA/ELRA model is solved using the Galerkin method of weighted residuals [*Parizek*, 2000, 2003].

Flexural deviatoric stresses are estimated from derivatives of the bedrock deflection profile (w) and a parameterization of elastic crustal thickness (T_{EC}), Young's modulus (E_{EC}), and Poisson's ratio (ν). Horizontal deviatoric stresses $\left(\sigma'_{xx}\right)$ are calculated from the concavity of the deflection profile [*Turcotte and Schubert*, 1982]:

$$\sigma'_{xx} = \left[\frac{E_{\text{EC}}}{(1-\nu^2)} \frac{\partial^2 w}{\partial x^2} \left(z + \frac{T_{\text{EC}}}{2} \right) \right] - \sigma_{xx,o} \tag{6}$$

where $\frac{\partial^2 w}{\partial x^2}$ is the concavity of the deflection profile, w, $\sigma_{xx,o}$ the initial stress state calculated from $b_{r,o}$, and z the depth with respect to the bedrock profile, b_r, where z is negative downward and referenced to a sea-level (SL) datum. This equilibrium profile is based on modern bedrock topography and ice thickness profiles and restored at the start of each simulation using that simulation's ELRA parameterization. Although this bending plate theory assumes shear stresses to be zero, an approximation of vertical differential shear stress can be calculated by integrating the horizontal deviatoric stress field over depth [*Timoshenko and Woinowsky-Krieger*, 1959]:

$$\tau'_{xz} = \left[\frac{E_{\text{EC}}}{2(1-\nu^2)} \frac{\partial^3 w}{\partial x^3} \left(z + \frac{T_{\text{EC}}}{2} \right)^2 \right] - \tau_{xz,o} \tag{7}$$

where $\frac{\partial^3 w}{\partial x^3}$ is the aberrance of the deflection profile and $\tau_{xz,o}$ the initial stress state calculated from the aberrance of $b_{r,o}$. As the sense of shear is unimportant to the direction of migration, the magnitude of the deviatoric vertical shear, $\left|\tau'_{xz}\right|$, is presented in our simulations.

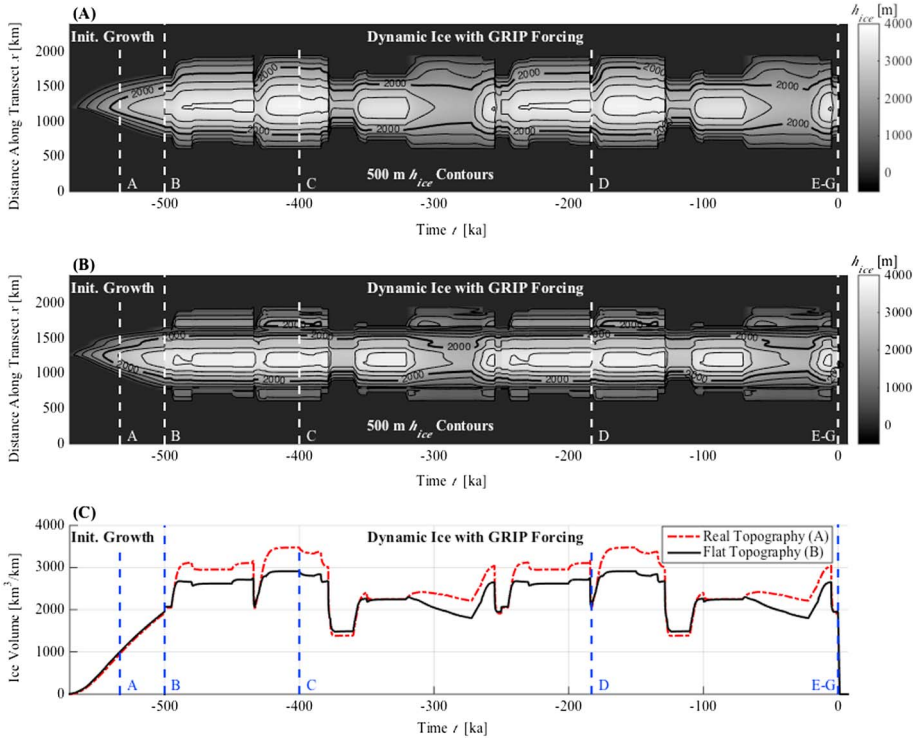

Figure 2. Dynamic ice-sheet thickness through time for our SEP on (a) flat bedrock and (b) realistic bedrock topography. (c) Ice volume through time for the simulation in Figure 2a (red) and Figure 2b (black). Key time slices, A through G, are shown for reference (white dashed lines in Figures 2a and 2b and blue in Figure 2c), and the major phases (Initial Growth and Dynamic Ice with GRIP Forcing) are labeled. The final decay and isostatic reequilibration occur following the E-G reference line and are fast enough to appear almost instantaneous at this scale.

2.2. Ice-Sheet Model Parameterization

Greenland's ice sheet has grown and shrunk with ice-age cycling and likely largely or completely deglaciated and reglaciated one or more times after initially forming [see *Alley et al.*, 2010]. To explore this range of behavior, we prescribe slow ice growth from initially deglaciated conditions, followed by two 110,000 year cycles driven by the GRIP ice-isotopic temperature record and proceeding to the modern as in prior work [*Parizek*, 2000, 2003; *Parizek and Alley*, 2004; *Parizek et al.*, 2005]. A rapid (~1.4 kyr) and complete ice-sheet decay is then forced, based on an extreme future warming scenario, and the model is run until the unloaded equilibrium bedrock profile ($b_{r,o}$) is reattained. The initial growth phase of each model run is based on a reversed and fiftyfold stretched version of the final decay, resulting in an ~70 kyr initial growth phase [*Parizek and Alley*, 2004]. Ice-sheet model dynamic forcing parameters are based on earlier work, with prescribed profiles of $\dot{A}$, $\dot{B}$, and A_o along the transect and through time, and the enhancement factor $F_{ice} = 15$ here, tuned to replicate results from the climate-based GrIS reconstructions using the GRIP ice-isotopic temperature proxy [*Parizek*, 2000; *Parizek and Alley*, 2004; *Parizek et al.*, 2005]. The sliding coefficient C was set to 1×10^{-8} m s^{-1} Pa^{-2} where and when $\dot{B} > 0$ m a^{-1} and to 0 where and when $\dot{B} \leq 0$ m a^{-1}. Ice-sheet model dynamic forcing parameterizations ($\dot{A}$, $\dot{B}$, and A_o) and final decay thinning rate data are detailed in the supporting information.

2.3. Earth Model Parameterization

We start with a standard elastic parameterization (SEP) Earth model and then perturb parameters through broad ranges around the preferred values. Lithospheric flexural rigidity in GrIS models generally has been taken to fall in the range 1×10^{24} to 1×10^{25} N m, but values as low as ~10^{23} N m and as high as ~10^{26} N m have been estimated from postglacial response, and more extreme values may occur locally [*McConnell*, 1968; *Wolf*, 1987; *Stern and Ten Brink*, 1989; *Fjeldskaar*, 1997; *Parizek and Alley*, 2004; *Rogozhina et al.*, 2012]. We start with rigidity $D_{lith} = 5 \times 10^{24}$ N m and test values from 1×10^{23} N m to 1×10^{26} N m. We follow the "quartz" crustal rheology of *Kohlstedt et al.* [1995], starting with Young's modulus $E_{EC} = 60$ GPa in our SEP, but test 40 to 80 GPa [*Turcotte and*

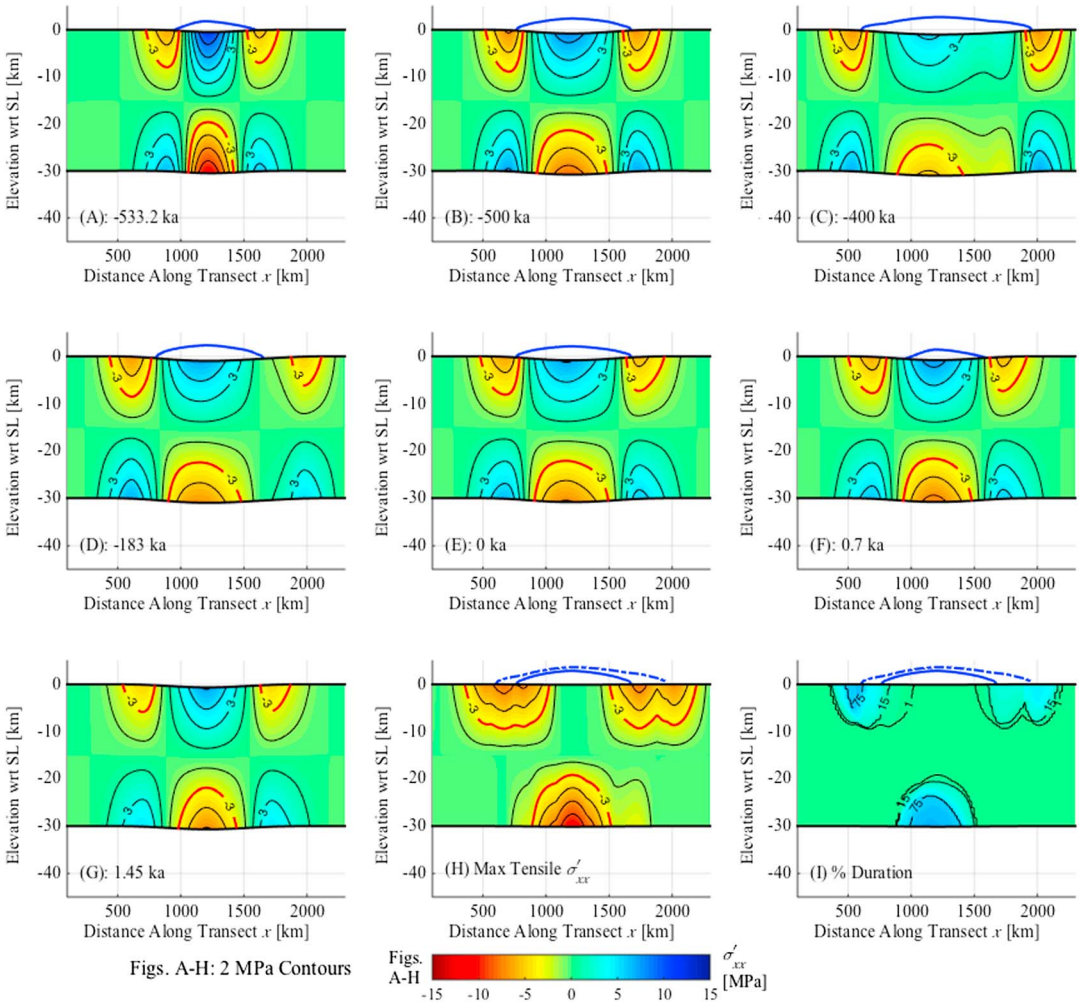

Figure 3. Flexure-induced horizontal deviatoric stresses (σ'_{xx}) for the SEP Earth model with initially flat bedrock. (a–g) Important time slices described in the text. (h) Maximum tensile stress at each point during the simulation and (i) the percent of the model run duration for which a point had tensile σ'_{xx} magnitudes ≥3 MPa (red contour in Figures 3a–3h), with longer durations marked by greater blue saturation, representing more time spent at or above threshold stresses that significantly contribute to dike migration of magmas. Ice extent in each time slice (Figures 3a–3g) is shown (blue) atop the elastic crustal profile, and in Figures 3h and 3i the modern (solid blue) and Last Glacial Maximum (LGM, dashed blue) ice extents are shown atop the unloaded equilibrium bedrock profile.

Schubert, 1982; *Burov and Diament*, 1995; *Kohlstedt et al.*, 1995]. We set the elastic thickness T_{EC} to 30 km along the entire profile, and explore values 10 km to 50 km, based on prior studies [*Maggi et al.*, 2000; *Shapiro and Ritzwoller*, 2004; *Fox-Maule et al.*, 2005, 2009; *McKenzie et al.*, 2005; *Braun et al.*, 2007]. We also test a spatially varying elastic thickness, setting the base of the elastic layer to be coincident with the 580°C isotherm from *Fox-Maule et al.* [2005], with a cubic interpolation of these Curie depth data. We set Poisson's ratio $v = 0.25$ [*Turcotte and Schubert*, 1982; *Kohlstedt et al.*, 1995].

3. Results

Ice-sheet thickness profiles through time are shown in Figure 2 for ice-sheet models coupled to the SEP Earth model with flat (Figure 2a) and realistic (Figure 2b) initial bedrock topography. Ice-sheet "volumes" ($km^3\ km^{-1}$ transect width) are also shown for these topographies (Figure 2c). The ice load is concentrated in central regions and on the continental shelves during glacial periods. Following earlier studies, we institute a crude "calving criterion" such that ice is not permitted to advance beyond the edge of the continental shelf, defined here as modern bathymetry deeper than −395 m with respect to sea level [e.g., *Parizek and Alley*, 2004].

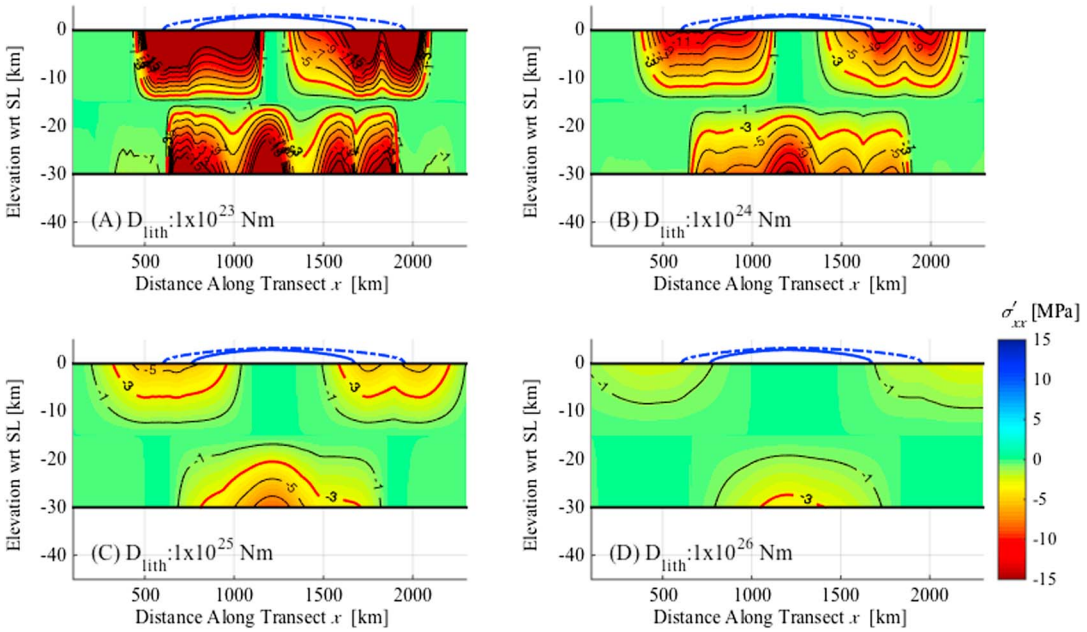

Figure 4. Maximum tensile σ'_{xx} magnitudes for simulations with varied D_{lith} from the SEP Earth model and flat bedrock topography, with D_{lith} of (a) 1×10^{23} N m, (b) 1×10^{24} N m, (c) 1×10^{25} N m, and (d) 1×10^{26} N m. Modern (solid) and LGM (dashed) ice extents are shown atop elastic crustal profiles. Threshold stresses for significant influence on dike migration ($\sigma'_{xx} \leq -3$ MPa) are shown as red contours.

Figure 3 presents our "standard simulation" with flat initial bedrock topography and the SEP Earth model. Sensitivities of the stress estimates from Figure 3 to key parameters are explored in subsequent figures: Figure 4 for D_{lith}, Figure 5 for E_{EC}, and Figure 6 for laterally uniform T_{EC}. Realistic bedrock topography influences modeled ice-sheet dynamics; thus, we assess the impacts of topographic variations against our flat standard simulation in Figure 7 and varying elastic crustal thickness (from Figures 1b and 1c) in Figures 8 and 9. Estimates of flexural deviatoric stresses are displayed with negative (tension) values of σ'_{xx} shown by warm colors in Figures 3–8 and higher values of $|\tau'_{xz}|$ shown by warm colors in Figure 9. As noted above, we consider tensile $\sigma'_{xx} \leq -3$ MPa and $|\tau'_{xz}| \geq 0.3$ MPa to be useful benchmarks, so we highlight these with red contours in Figures 3–9.

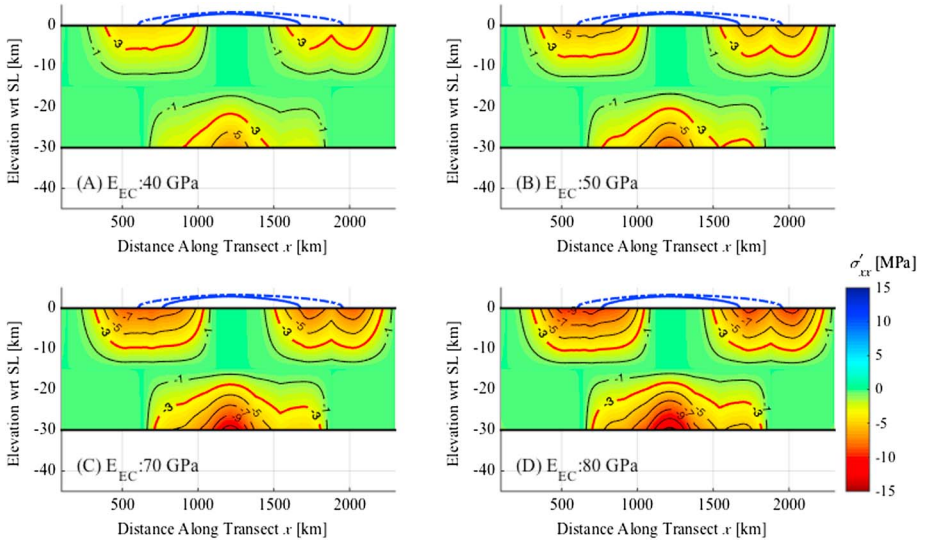

Figure 5. Maximum tensile σ'_{xx} magnitudes for simulations with varied E_{EC} from the SEP Earth model and flat bedrock topography, with E_{EC} of (a) 40 GPa, (b) 50 GPa, (c) 70 GPa, and (d) 80 GPa. Modern (solid) and LGM (dashed) ice extents are shown atop elastic crustal profiles. Threshold stresses for significant influence on dike migration ($\sigma'_{xx} \leq -3$ MPa) are shown as red contours.

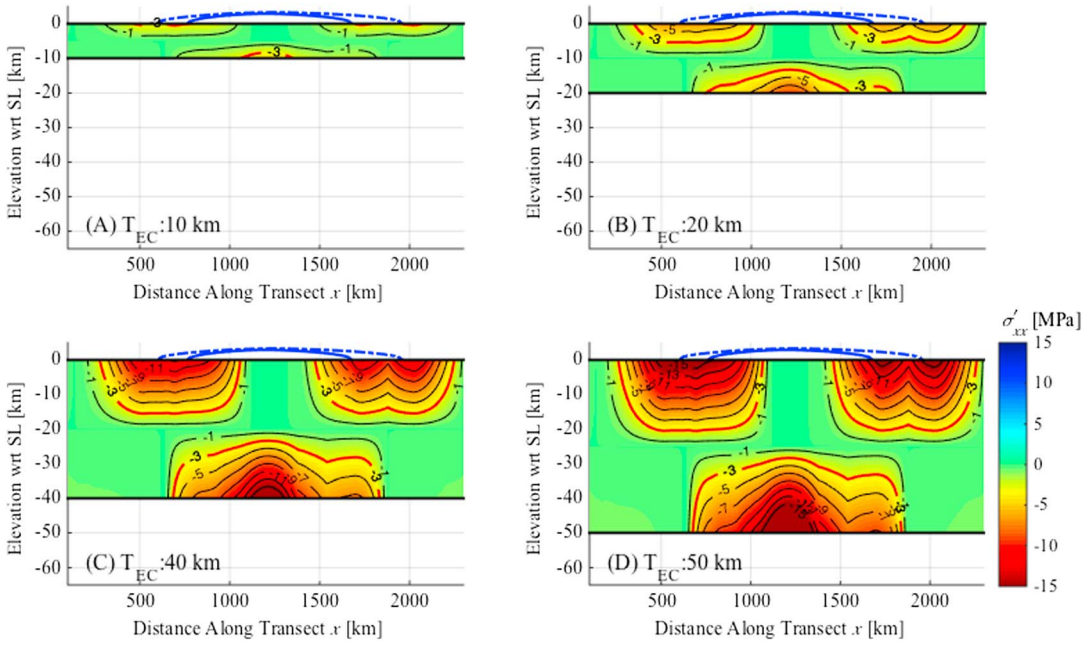

Figure 6. Maximum tensile σ'_{xx} amplitude for simulations with varied, uniform T_{EC}, from the SEP Earth model and flat bedrock topography, with T_{EC} of (a) 10 km, (b) 20 km, (c) 40 km, and (d) 50 km. Modern (solid) and LGM (dashed) ice extents are shown atop elastic crustal profiles. Threshold stresses for significant influence on dike migration ($\sigma'_{xx} \leq -3$ MPa) are shown as red contours.

In addition, Figures 3, 8, and 9 show important time slices: (a) the midpoint of the growth phase, when ice volume is one half of the modern ice volume (circa 533 ka); (b) the end of the growth phase, when ice volume equals modern ice volume (circa 500 ka); (c) a glacial maximum after additional, slow ice-sheet growth (circa 400 ka); (d) following a rapid deglaciation, when ice volume is roughly equal to modern (circa 183 ka); (e) modern, after additional ice-age cycling and the persistence of warm conditions during the Holocene (0 ka); (f) midpoint of rapid removal of GrIS when ice volume is one half of modern ice volume (circa 700 annum in the future); and (g) immediately after full removal of GrIS but before full postglacial isostatic adjustment (circa 1450 annum in the future). The largest stress favoring melt migration achieved during the full simulation is contoured in Figures 3h, 8h, and 9h, and the total time that the stress magnitude exceeds our benchmark stress is contoured in Figures 3i, 8i, and 9i.

3.1. Standard Simulation

Many features of the simulations are seen most clearly in the flat-topography constant-lithospheric-thickness runs (Figure 3). Ice-sheet loading depresses the central part of the lithosphere and forms peripheral forebulges. The upper crust is placed under horizontal compression in the central regions and tension in the forebulges, with similar magnitude but opposite sign stresses in the lower crust, mirrored about a neutral axis (see Figures 3a–3g). The stress pattern migrates outward with ice-sheet growth and inward with decay (most clearly shown in Figures 3b–3e). During glacial maxima, the ice extent exceeds the characteristic wavelength of lithospheric deflection, causing the central region of the depression to flatten and splitting the central stress extremes into two centers closer to the margins (Figure 3c) [see *Brotchie and Silvester*, 1969; *Turcotte and Schubert*, 1982]. Stress magnitudes are smaller under smaller ice-sheet loads, so regions experiencing multi-MPa tensile stresses in the forebulge do not migrate as far as the ice-sheet margins do (Figure 3h; also compare Figures 3c and 3f). During rapid, complete deglaciation, stress maxima decay with little lateral migration (Figures 3e–3g) as the lithosphere approaches unloaded equilibrium. High stresses persist for a large fraction of the total simulation length (compare Figures 3h and 3i). Ice-sheet volumes are larger than modern for most of the experiment, consistent with the relatively reduced interglacial state of the modern GrIS.

3.2. Model Sensitivity Simulations

We next assess sensitivity of the results from our standard simulation (Figure 3) to single-parameter variations from the SEP and initial bedrock topography. We display the maximum tensile σ'_{xx} magnitudes attained

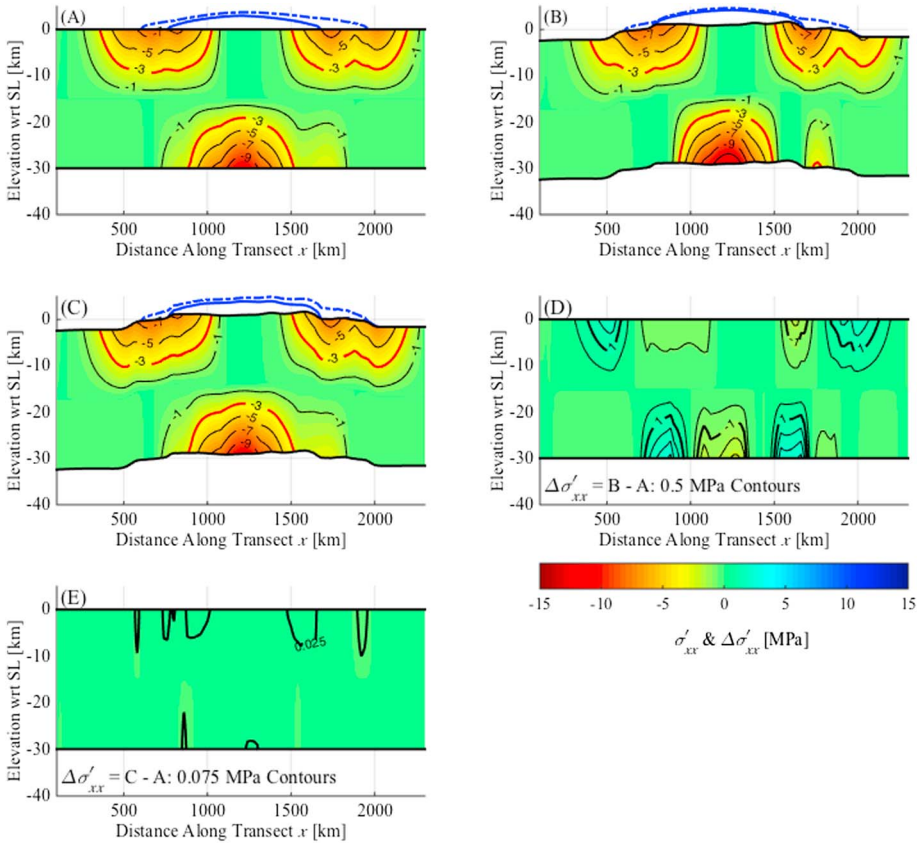

Figure 7. Comparison of the effects of topographic focusing and ice mass redistribution on the amplitude of the maximum tensile σ'_{xx} for simulations with the SEP Earth model. Maximum tensile stresses are shown for (a) flat initial topography and (b) realistic topography in response to identical ice-sheet loading histories (as in Figure 3) and (c) realistic topography in response to a dynamically responsive ice-sheet load. Stress fields are differenced to examine (d) stress focusing (Figure 7a subtracted from Figure 7b) and (e) overall (Figure 7a subtracted from Figure 7c) effects of incorporating realistic initial topography. Threshold stresses for significant influence on dike migration ($\sigma'_{xx} \leq -3$ MPa) are shown as red contours in Figures 7a–7c.

during each simulation (as in Figure 3h), for D_{lith} between 1×10^{23} N m and 1×10^{26} N m (Figure 4), E_{EC} between 40 GPa and 80 GPa (Figure 5) and T_{EC} between 10 km and 50 km (Figure 6). Figure 7 compares maximum tensile σ'_{xx} magnitudes for flat and realistic bedrock topography for the SEP Earth model.

Lithospheric flexural rigidity likely depends on a number of factors including strain rate, thermal structure, and composition and may change over time [*Burov and Diament*, 1992, 1995; *Kohlstedt et al*., 1995; *Maggi et al*., 2000; *McKenzie et al*., 2005]. Figure 4 shows that increasing flexural rigidity distributes flexural response over longer distances with less curvature and therefore smaller deviatoric stresses. However, even with the highest rigidity tested, tensile σ'_{xx} magnitudes still exceed 3 MPa, our target stress for significant cryospheric contribution to magma migration via dike formation, beneath the central ice-sheet region. Though not shown here, decreasing the asthenospheric flow constant τ_{asth} would lead to larger stress magnitudes that sweep farther and more rapidly in response to ice-margin migration.

Flexural deviatoric stresses in the crust are calculated from the deflection of the lithosphere and mechanical properties of the elastic crust. As shown in equations (6) and (7), σ'_{xx} and $|\tau'_{xz}|$ for a given deflection increase linearly with E_{EC}. This behavior is evident in maximum tensile σ'_{xx} in Figure 5. Even for the lowest E_{EC} value tested, maximum tensile σ'_{xx} magnitudes exceed 3 MPa in many places.

Similarly, σ'_{xx} magnitudes increase linearly with greater T_{EC}, as indicated by equation (6), and shown in the T_{EC} sensitivity simulations in Figure 6. Equation (7) indicates a quadratic relationship between T_{EC} and $|\tau'_{xz}|$, and while not explicitly shown here, this trend can be observed in the GRIP transect simulation (Figure 9).

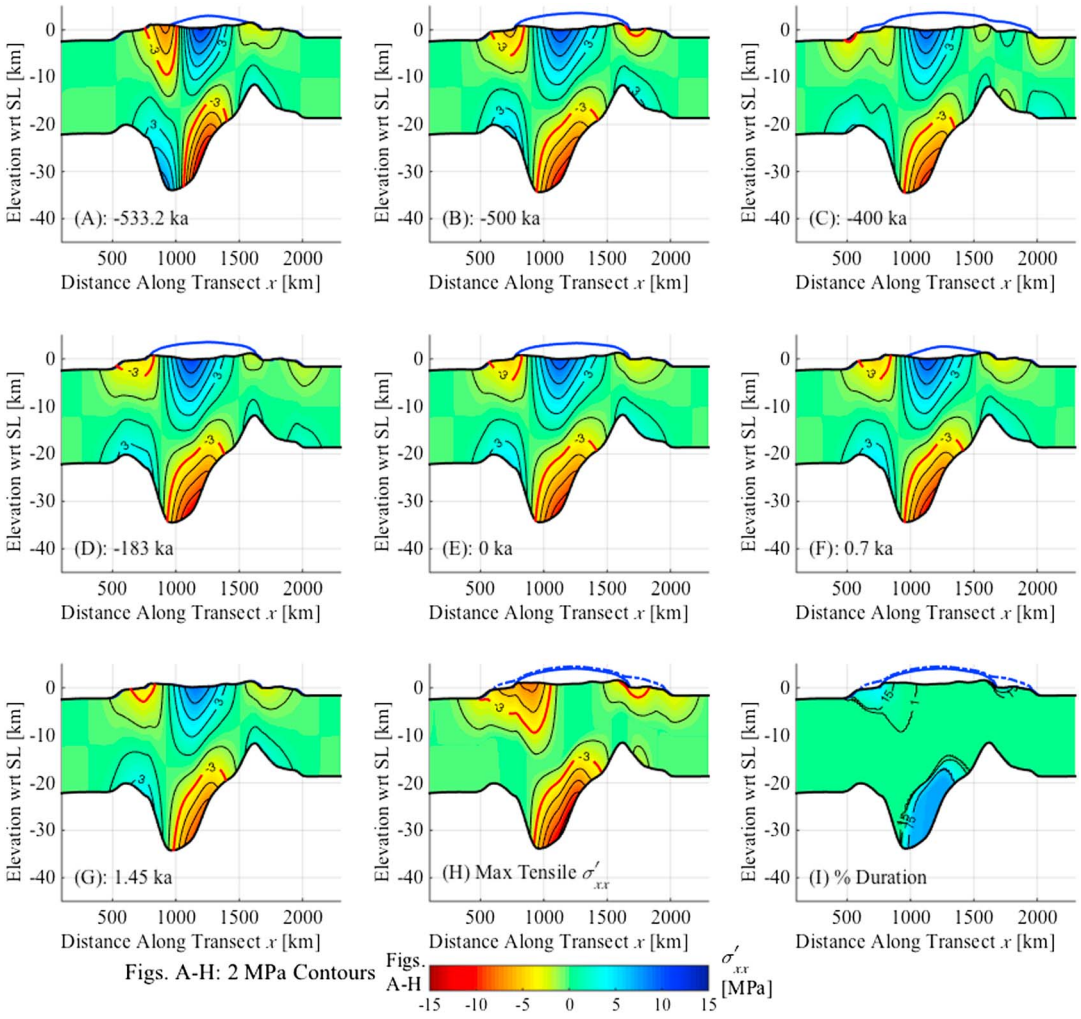

Figure 8. Flexure-induced σ'_{xx} for the parameterized GRIP transect topography and variable T_{EC} estimates (from Figure 1c) with the SEP Earth model. (a–g) The same time slices as Figures 3a–3g. (h) The maximum tensile σ'_{xx} amplitude and (i) the percent of the total time simulated that tensile stress magnitudes ≥3 MPa (red contour in Figures 8a–8h as in Figures 3h and 3i).

As shown in Figure 7, incorporating actual topography (from Figure 1c) into our standard simulation produces marked changes in stress magnitudes and distribution. Changing initial topography without changing the load will affect flexural stresses through focusing, but changing topography also affects ice dynamics and thus the ice loading profile. To separate these effects, we show the maximum tensile σ'_{xx} from the standard simulation (Figure 7a), the stresses resulting from placing that ice sheet on real topography (Figure 7b), and the stresses from the ice-sheet interacting with the real topography (Figure 7c). The effect of the topography alone is shown in Figure 7d, where the values from Figure 7a are subtracted from Figure 7b, producing stress changes typically less than 0.1 MPa and thus small compared to the flexural stresses. The full effects of the realistic topography are shown in Figure 7e, which subtracts Figure 7a from Figure 7c, perturbing tensile stress magnitudes as much as 5 MPa in some places but generally less than 3 MPa. These results show that the main effect of this realistic topography is to perturb ice mass distribution rather than to focus stresses. We note, however, that somewhat larger but shorter-lived stress concentrations are generated by the topography in certain times and places, suggesting the possibility that careful considerations of ice-sheet interactions with more extreme topography might reveal interesting effects.

3.3. GRIP Transect Simulations

Geophysical evidence suggests notable thickness variations in the elastic crust across the study area [*Maggi et al.*, 2000; *Fox-Maule et al.*, 2005; *McKenzie et al.*, 2005; *Braun et al.*, 2007; *Petrunin et al.*, 2013], and we

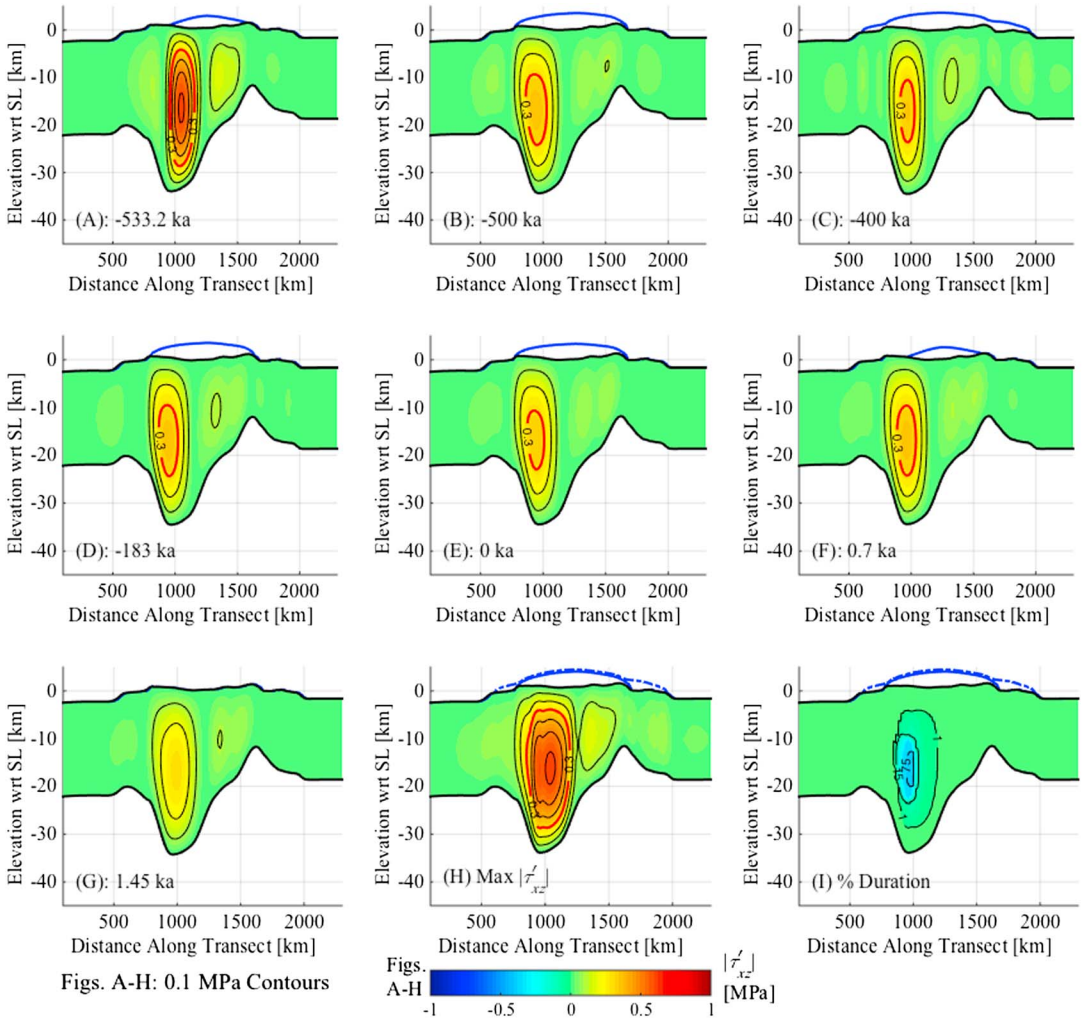

Figure 9. Flexure-induced $|\tau'_{xz}|$ for the parameterized GRIP transect topography and variable T_{EC} estimates (from Figure 1c) with the SEP Earth model. (a–g) The same time slices as Figures 3a–3g. (h) The maximum $|\tau'_{xz}|$ and (i) the percent of the total time simulated that stress magnitudes ≥0.3 MPa (red contours in Figures 9a–9h) during the simulation as in Figures 3h and 3i.

implement this in Figures 8 and 9. Following previous studies, we vary elastic crustal thickness while holding other elastic properties constant acknowledging that the lithosphere's resistance to bending under an applied load, and by extension the differential stresses, may not vary as a function of only one parameter [see *Burov and Diament*, 1992, 1995; *Kohlstedt et al.*, 1995; *Parizek*, 2000, 2003; *Parizek and Alley*, 2004; *Rogozhina et al.*, 2012]. Consistent with equations (6) and (7), the largest tensile σ'_{xx} in Figure 8 and largest $|\tau'_{xz}|$ in Figure 9 occur in the thickest regions of crust. Maximum tensile σ'_{xx} magnitudes exceed 10 MPa. Introducing varied crustal thickness shifts the deep, central stress maxima toward the thickness maximum. Furthermore, interactions between the evolving ice sheet and the spatially varying crustal thickness enhance stress magnitudes in some regions and diminish them in others compared to earlier simulations. Note, for example, the strong but short-lived stress maxima in the western part of the transect and weakened stress maxima in the eastern part (compare Figures 8h and 8i with Figures 3h and 3i).

As indicated by equation (7), Figure 9 shows that $|\tau'_{xz}|$ maxima are strongly affected by variable T_{EC}, concentrating in the thickest crustal regions, and only weakly affected by ice-sheet extent. The largest $|\tau'_{xz}|$ simulated are in excess of 0.5 MPa, although this occurs almost exclusively at the onset of glaciations (Figure 9a). During dynamic ice-sheet cycling, $|\tau'_{xz}|$ maxima typically do not exceed 0.3 MPa. Stresses of these magnitudes are long lived in the thickest parts of the crust (Figure 9i) and do reside above the lower threshold suggested to induce vug-wave style migration in select settings [see *Phipps Morgan and Holtzman*, 2005].

3.4. Summary of Model Results

These flowline simulations with a well-characterized ice-flow model coupled to an ELRA Earth model show that ice-age cycling in Greenland forces large elastic and viscous responses in the Earth beneath and nearby.

All simulations generate σ'_{xx} of sufficient magnitude to notably affect dike formation in magmatic systems [*Cooper*, 1990; *Rubin*, 1995a, 1995b]. The greatest σ'_{xx} magnitudes develop in the upper elastic crust beneath forebulges around the ice sheet, and tensile maxima in the lower crust reside in central regions beneath the ice-sheet load. Topographic features cause marked changes in ice-sheet load distribution, resulting in stress-field focusing beneath dynamically thickened ice. Likewise, crustal thickness variations concentrate stresses in thicker regions in our simulations.

Simulated stress fields migrate as ice-sheet oscillations cause forebulges and associated stresses to move laterally and the central depression to expand and contract. Migration of these stress patterns notably lags faster ice-volume changes because of viscous asthenospheric flow resistance, most notably during rapid ice-sheet decay. The details of stress-state evolution thus depend on the rate of ice-sheet change, although the size and thickness of the ice-sheet are generally more important than the rate of ice-volume oscillation in controlling tensile and shear stress magnitudes that can impact magma migration or shallow crustal fracturing. The largest variations in stress-field distribution occur at the onset of the initial glaciation and final deglaciation; however, ice-age cycling between glacial and interglacial (but not deglaciated) periods is sufficient to generate large stress changes.

We further note that decreasing τ_{asth} would tend to sweep the high-stress zones across a broader region. As the time for bedrock compensation is diminished, the stress state captures more relatively rapid load fluctuations (e.g., on final deglaciation the stress changes would sweep farther inland, rather than slowly fading away in place). Conversely, increasing τ_{asth} would tend to localize the high-stress regions within areas where the load was relatively constant for long periods, with quicker fluctuations effectively filtered by the slower response times. This follows because the elastic lithosphere (equation (1)) dictates the shape of the isostatically compensated profile, while the relaxed asthenosphere (equation (2)) dictates the rate at which it approaches that new equilibrium deflection. If load changes are fast compared to asthenospheric flow, deflection profiles (and therefore stress changes) are time limited, whereas if load changes are relatively slow, deflection profiles are load limited. For reasonable values of τ_{asth}, the differences would be most pronounced for periods of rapid changes, as τ_{asth} dictates whether stress changes sweep across the domain or not.

Regardless of the details of stress migration, we find across our broad parameter space that stresses are strongly tensile in widespread regions for well over 10% of an ice-age cycle. Consistent with underlying flexural physics, modeled tensile stresses remain small at middepths. However, significant vertical shear stress maxima are simulated in some regions, which span middepths and are of sufficient magnitude that they may enhance magma migration via vug-waves or other mechanisms.

4. Discussion and Conclusions

The effects of ice-sheet oscillations on lithospheric stresses beneath GrIS are large, even without the potentially significant additional impact of glacier erosion, sediment transport, and deposition on the loading history [*Sternai et al*., 2016]. For comparison, the melting of a 3 km ice sheet over 10 ka, a typical rate of deglaciation [*Shackleton et al*., 1984; *Alley et al*., 2010], changes loading at roughly the same rate as unloading of crustal rock at 10 cm a^{-1} over a continental-scale area and at rates far higher than sea-level oscillations, which are thought to appreciably influence magma extraction at mid-ocean ridge [e.g., *Crowley et al*., 2015]. Numerous studies have shown that the direct effects of loading, and the resultant flexure, significantly affect brittle crustal processes and shallow magmatism [*Wu and Hasegawa*, 1996; *Stewart et al*., 2000; *Hampel and Hetzel*, 2006; *Llubes et al*., 2006; *Huybers and Langmuir*, 2009]. Observed, unexpectedly high GHF beneath ice-sheet regions led to the hypothesis that oscillatory loading from ice-age cycling contributed to enhanced GHF by one or several processes including enhancement of magma extraction from deep rocks, magma migration into shallower locations (or completely through) the lithosphere, or deep groundwater flow accessing hot rocks and communicating with shallow subglacial hydrologic systems. In this study, we quantitatively investigate the hypothesis that GHF anomalies beneath the GrIS may be explained by shallowly emplaced magma and/or hydrothermal circulation enhanced by flexure-induced lithospheric stresses from

cyclic ice-sheet loading, drawing upon the theories and observations of many previous studies [*Hall*, 1982; *Hardarson and Fitton*, 1991; *Sigvaldason et al*., 1992; *Zielinski et al*., 1994, 1996; *Fahnestock et al*., 2001; *Dahl-Jensen et al*., 2003a; *Huybers and Langmuir*, 2009].

The first ice age after a long interval with no ice will suppress melt volume by raising the pressure melting point at depth. However, under some circumstances, a sufficiently long interval of ice-age cycling and the resulting erosion may cause the system to become insensitive to conditions before the initial glaciations. If so, then cyclic loading will cause a roughly linear oscillation in melt fraction and a quadratic increase in extraction efficiency during deglaciations (unloading) [e.g., *McKenzie*, 1984; *Kohlstedt and Holtzman*, 2009]. Larger-amplitude loading variations will increase the ability of melt to migrate, potentially forming magma bodies that otherwise would not form [see *Huybers and Langmuir*, 2009]. Subglacial erosion further reduces loading, causing additional melting [*Sternai et al*., 2016]. Our results support this hypothesis, but much work is still necessary to quantify this effect for specific locations.

Buoyant melt rises through the crust by many processes but is clearly aided by emplacement of largely vertical dikes in many cases [e.g., *Ahern and Turcotte*, 1979; *Rubin*, 1995a, 1995b; *Burov et al*., 2003]. Stresses necessary for dike propagation can arise from tectonic processes, source-region overpressure, or other mechanisms. Our modeling suggests that for a broad range of crustal parameterizations, ice-age cycling of Greenland's ice sheet generates deviatoric tensile stresses of similar magnitude to those required for dike propagation. Shallow tensile stress maxima migrate laterally in the crust largely in response to ice-sheet margin dynamics, likely favoring volcanism sourced from existing shallow magma bodies [e.g., *Hall*, 1982; *Huybers and Langmuir*, 2009, and references therein]. The strongest, longest-lived tensile stresses in our simulations are deep maxima beneath central ice-sheet regions, which tend to change in magnitude in response to cyclic loading and favor dike emplacement at depth.

In some locations and conditions, relatively large differential shear stresses develop and extend across the middepth crust, suggesting that shear-related magma migration processes could enhance upward magma migration from the lower crust [*Phipps Morgan and Holtzman*, 2005]. The pattern and magnitude of stresses change in response to ice-sheet evolution, increasing the likelihood that a preexisting magma body beneath or near Greenland would encounter favorable conditions for upward migration. Our simulations do not show conditions that would favor a single-step (or single-process) migration from beneath the lower crust to the surface, but the combination of processes explored here (and potentially others) could result in a multistep enhancement of magma ascent via glaciotectonic stresses, as illustrated by overlap of significant, deviatoric tensile (Figure 8h) and shear (Figure 9h) stress fields. Shallow glaciotectonic stresses, modeled here to be tensile within regions closely tied to the forebulge, likely affect shallow crustal processes, and if buoyant melt is present beneath, they must affect the likelihood or rate of magma ascent. Simulated stress-field migration in response to ice-sheet evolution suggests multiple opportunities for migration of magmas in some regions, with multistep migration possible beneath and near the GrIS.

Additionally, shallow glaciotectonic stresses likely aid in shallow crustal fracturing and faulting (see review by *Stewart et al*. [2000]). If this enhances shallow permeability of the crust and exceeds permeability loss from glacially induced erosion, then ice-age cycling might aid enhanced penetration of subglacial hydrothermal systems, thereby enhancing GHF beneath ice sheets [*Clark and Pollard*, 1998; *Llubes et al*., 2006; *Huybers and Langmuir*, 2009; *Sternai et al*., 2016].

Combining our stress modeling results with earlier studies, we consider it likely that under appropriate conditions ice-age cycling does increase GHF to some regions beneath ice sheets. In turn, this suggests that some long-term changes in ice-sheet size and behavior result from interactions with the lithosphere and thus that the climatic history of ice-age cycling has been affecting geologic processes [*Clark and Pollard*, 1998; *Huybers and Langmuir*, 2009; *Crowley et al*., 2015; *Sternai et al*., 2016]. In addition, we suggest that these processes are not limited to Greenland but could be as important, or more important, in West Antarctica and perhaps elsewhere [*Llubes et al*., 2006; *Huybers and Langmuir*, 2009; *Paulsen and Wilson*, 2010; *Schroeder et al*., 2014].

A large gap exists between these considerations and any quantitative test of the hypothesis that GHF anomalies in Greenland arose in part from the influence of the ice-sheet growth and decay over climatic cycles. We quantitatively demonstrate that deviatoric stresses from ice-sheet loading simulations are sufficiently large to meaningfully contribute to upward migration of subjacent magmas in a number of reasonable model parameterizations. The preglacial passage of the Iceland-Jan Mayen hot spots beneath Greenland provides the

possibility of a source of magma at depth and thinned lithosphere, shortening magma ascent distances [*Lawver and Müller*, 1994; *Braun et al*., 2007, and references therein; *Rogozhina et al*., 2016] and perhaps contributing to the variations in elastic thickness that focus stresses and make melt migration more likely. Ongoing research is revealing connections between glacial and magmatic processes [e.g., *Crowley et al*., 2015; *Sternai et al*., 2016; *Rogozhina et al*., 2016], but additional work is required to fully test the hypotheses presented here. We believe that our findings motivate higher-order modeling and targeted geophysical studies over GHF anomalies beneath the Greenland ice sheet and other ice sheets.

Acknowledgments
We thank the National Science Foundation (NSF) for support under grants including CReSIS 0424589, AGS-1338832, and PLR-1443190 and the National Aeronautics and Space Administration (NASA) for support under grants NNX-10-AI04G and NNX-15-AH84G. We thank K.P. Furlong and S. Anandakrishnan for their helpful discussions on the development of this study and three reviewers for their insightful comments and suggestions. Data implemented in this study are available from NASA [*Fox-Maule et al*., 2005] and NOAA [*Amante and Eakins*, 2009], and results reported here can be obtained from the first author (nate.t.stevens@gmail.com).

References

Ahern, J. L., and D. L. Turcotte (1979), Magma migration beneath an ocean ridge, *Earth Planet. Sci. Lett.*, *45*, 115–122.
Alley, R. B., et al. (2010), History of the Greenland ice Sheet: Paleoclimatic insights, *Quat. Sci. Rev.*, *80*(3), 1728–1756, doi:10.1016/j.qascirev.2010.02.007.
Amante, C., and B. W. Eakins (2009), ETOPO1 1 Arc-Minute Global Relief Model: Procedures data sources and analysis, NOAA Tech. Memo. NESDIS NGDC-24, Nat. Geophys. Data Cent., NOAA, doi:10.7289/V5C8276M.
Braun, A., H. R. Kim, B. Csatho, and R. R. B. von Frese (2007), Gravity-inferred crustal thickness of Greenland, *Earth Planet. Sci. Lett.*, *262*, 138–158, doi:10.1016/j.epsl.2007.07.050.
Brotchie, J. F., and R. Silvester (1969), On crustal flexure, *J. Geophys. Res.*, *100*, 3905–3927, doi:10.1029/JB074i22p05240.
Burov, E. B., and M. Diament (1992), Flexure of the continental lithosphere with multilayered rheology, *Geophys. J. Int.*, *109*, 449–468, doi:10.1111/j.1365-246X.1992.tb00107.x.
Burov, E. B., and M. Diament (1995), The effective elastic thickness (Te) of continental lithosphere: What does it really mean?, *J. Geophys. Res.*, *100*, 3905–3927, doi:10.1029/94JB02770.
Burov, E. B., C. Jaupart, and L. Guillou-Frottier (2003), Ascent and emplacement of buoyant magma bodies in brittle-ductile upper crust, *J. Geophys. Res.*, *108*(B4), 2177, doi:10.1029/2002JB0001904.
Clark, P. U., and D. Pollard (1998), Origin of middle Pleistocene transition by ice sheet erosion of regolith, *Paleoceanography*, *13*(1), 1–9, doi:10.1029/97PA02660.
Connolly, J. A. D., M. W. Schmidt, G. Solferino, and N. Bagdassarov (2009), Permeability of asthenospheric mantle and melt extraction rates at mid-ocean ridges, *Nature*, *462*, 209–213, doi:10.1038/nature08517.
Cooper, R. F. (1990), Differential stress-induced melt migration: An experimental approach, *J. Geophys. Res.*, *95*, 6979–6992, doi:10.1029/JB095iB05p06979.
Crowley, J. W., R. F. Katz, P. Huybers, C. Langmuir, and S.-H. Park (2015), Glacial cycles drive variations in the production of oceanic crust, *Science*, *347*(6227), 1237–1240, doi:10.1126/science.1261508.
Cuffey, K. M., and W. S. B. Patterson (2010), *The Physics of Glaciers*, 4th ed., Academic, Cambridge, Mass.
Dahl-Jensen, D., N. Gundestrup, S. P. Gogineni, and H. Miller (2003a), Basal melt at NorthGRIP modeled from borehole, ice-core and radio-echo sounder observations, *Ann. Glaciol.*, *37*, 207–212, doi:10.3189/172756403781815492.
Dahl-Jensen, T., T. B. Larsen, I. Woelbern, T. Bach, W. Hanka, R. Kind, S. Gregersen, K. Mosegaard, P. Voss, and O. Gudmundsson (2003b), Depth to Moho in Greenland: Receiver-function analysis suggests two Proterozoic blocks in Greenland, *Earth Planet. Sci. Lett.*, *205*, 379–393, doi:10.1016/S0012-821X(02)01080-4.
Ekholm, S., R. Forsberg, and J. M. Brozena (1995), Accuracy of satellite altimeter elevations across the Greenland ice sheet, *J. Geophys. Res.*, *100*, 2687–2696, doi:10.1029/94JC03042.
Fahnestock, M., W. Abdalati, I. Joughin, J. Brozena, and P. Gogineni (2001), High geothermal heat flow, basal melt, and the origin of rapid ice flow in central Greenland, *Science*, *294*(5550), 2338–2342, doi:10.1126/science.1065370.
Fjeldskaar, W. (1997), Flexural rigidity of Fennoscandia inferred from the postglacial uplift, *Tectonics*, *16*, 596–608, doi:10.1029/97TC00813.
Fox-Maule, C., M. E. Purucker, N. Olsen, and K. Mosegaard (2005), Heat flux anomalies in Antarctica revealed by satellite magnetic data, *Science*, *309*(5733), 464–467, doi:10.1126/science.1106888.
Fox-Maule, C., M. E. Purucker, and N. Olsen (2009), *Inferring Magnetic Crustal Thickness and Geothermal Heat Flux From Crustal Magnetic Field Models*, *Danish Clim. Cent. Rep.*, Danish Meteorol. Inst., Copenhagen.
Glen, J. W. (1955), The creep of polycrystalline ice, *Proc. R. Soc. A*, *288*, 519–538, doi:10.1098/rspa.1955.0066.
Greve, R. (2005), Relation of measured basal temperatures and the spatial distribution of the geothermal heat flux fo the Greenland ice sheet, *Ann. Glaciol.*, *42*, 424–432, doi:10.3189/172756405781812510.
Hall, K. (1982), Rapid deglaciation as an initiator of volcanic activity: An hypothesis, *Earth Surf. Processes Landforms*, *7*, 45–51, doi:10.1002/esp.3290070106.
Hampel, A., and R. Hetzel (2006), Response of normal faults to glacial-interglacial fluctuations of ice and water masses on the Earth's surface, *J. Geophys. Res.*, *111*, B06406, 1–13, doi:10.1029/2005JB004124.
Hardarson, B., and G. Fitton (1991), Increased mantle melting beneath Snaefellsjökull volcano during Late Pleistocene deglaciation, *Nature*, *353*, 62–64, doi:10.1038/353062a0.
Huybers, P., and C. Langmuir (2009), Feedback between deglaciation, volcanism, and atmospheric CO_2, *Earth Planet. Sci. Lett.*, *286*, 479–491, doi:10.1016/j.epsl.2009.07.014.
Huybrechts, P. (2002), Sea-level changes at the LGM from ice-dynamic reconstructions of the Greenland and Antarctic ice sheets during the glacial cycles, *Quat. Sci. Rev.*, *21*, 203–231, doi:10.1016/S0277-3791(01)00082-8.
Joughin, I., B. E. Smith, I. M. Howat, T. Scambos, and T. Moon (2010), Greenland flow variability from ice-sheet-wide-velocity mapping, *J. Glaciol.*, *56*(197), 415–430, doi:10.3189/002214310792447734.
Klemann, V., and D. Wolf (1998), Modelling of stresses in Fennoscandian lithosphere induced by Pleistocene glaciations, *Tectonophysics*, *294*, 291–303, doi:10.1016/S0040-1951(98)00107-3.
Kohlstedt, D. L., and B. K. Holtzman (2009), Shearing melt out of the Earth: An experimentalist's perspective on the influence of deformation on melt extraction, *Annu. Rev. Earth Planet. Sci.*, *37*, 561–593, doi:10.1146/annurev.earth.031208.100104.
Kohlstedt, D. L., B. Evans, and S. J. Mackwell (1995), Strength of the lithosphere: Constraints imposed by laboratory experiments, *J. Geophys. Res.*, *100*, 17,587–17,602, doi:10.1029/95JB01460.

Larour, E., M. Morlighem, H. Seroussi, J. Schiermeier, and E. Rignot (2012), Ice flow sensitivity to geothermal heat flux of Pine Island Glacier, Antarctica, *J. Geophys. Res.*, *117*, F04023, 1–12, doi:10.1029/2012JF002371.
Lawver, L., and R. Müller (1994), Iceland hotspot track, *Geology*, *22*, 311–314, doi:10.1130/0091-7613(1994).
Le Meur, E., and P. Huybrechts (1996), A comparison of different ways of dealing with isostasy: Examples from modelling the Antarctic ice sheet during the last glacial cycle, *Ann. Glaciol.*, *23*, 309–317.
Letréguilly, A., P. Huybrechts, and N. Reeh (1991), Steady state characteristics of the Greenland ice sheet under different climates, *J. Glaciol.*, *37*, 149–157.
Lliboutry, L. (1965) Traite' de glaciologie, Masson et Cie [in French], Paris.
Llubes, M., C. Lanseau, and F. Rémy (2006), Relations between basal condition, subglacial hydrological networks and geothermal flux in Antarctica, *Earth Planet. Sci. Lett.*, *241*, 655–662, doi:10.1016/j.epsl.2005.10.040.
Maggi, A., J. A. Jackson, D. McKenzie, and K. Priestley (2000), Earthquake focal depths, effective elastic thickness, and the strength of the continental lithosphere, *Geology*, *28*(6), 495–498, doi:10.1130/0091-7613(2000).
McConnell, R. K. (1968), Viscosity of the mantle from relaxation time spectra of isostatic adjustment, *J. Geophys. Res.*, *73*, 7089–7105, doi:10.1029/JB073i022p07089.
McKenzie, D. (1984), The generation and compaction of molten rock, *J. Petrol.*, *25*(3), 713–765, doi:10.1093/petrology/25.3.713.
McKenzie, D., and M. J. Bickle (1988), The volume and composition of melt generated by extension of the lithosphere, *J. Petrol.*, *29*(3), 625–679, doi:10.1093/petrology/29.3.625.
McKenzie, D., J. Jackson, and K. Priestley (2005), Thermal structure of oceanic and continental lithosphere, *Earth Planet. Sci. Lett.*, *233*, 337–349, doi:10.1016/j.epsl.2005.02.005.
Müller, R. D., J.–Y. Royer, and L. A. Lawver (1993), Revised plate motions relative to the hotspots from combined Atlantic and Indian Ocean hotspot tracks, *Geology*, *21*, 275–278, doi:10.1130/0091-7613(1993)021.
Parizek, B. R. (2000), Thermomechanical flowline model for studying the interactions between ice sheets and the global climate system, master's thesis, The Pennsylvania State Univ.
Parizek, B. R. (2003), Modeling the West Antarctic and Greenland Ice Sheets: New dynamic, thermodynamic, and isostatic insights, Doctoral Dissertation, The Pennsylvania State Univ., Univ. Park, Pa.
Parizek, B. R., and R. B. Alley (2004), Implications of increased Greenland surface melt under global-warming scenarios: Ice-sheet simulations, *Quat. Sci. Rev.*, *23*(9-10), 1013–1027, doi:10.1016/j.quascirev.2003.12.024.
Parizek, B. R., R. B. Alley, S. Anandakrishnan, and H. Conway (2002), Sub-catchment melt and long-term stability of ice stream D, West Antarctica, *Geophys. Res. Lett.*, *29*(8), 1214, doi:10.1029/2001GL014326.
Parizek, B. R., R. B. Alley, and C. L. Hulbe (2003), Subglacial thermal balance permits ongoing grounding-line retreat along the Siple Coast of West Antarctica, *Ann. Glaciol.*, *36*, 251–256, doi:10.3189/172756403781816167.
Parizek, B. R., R. B. Alley, and D. R. MacAyeal (2005), The PSU/UofC finite-element thermomechanical flowline model of ice-sheet evolution, *Cold Reg. Sci. Technol.*, *42*, 145–168, doi:10.1016/j.coldregions.2004.12.006.
Paulsen, T. S., and T. J. Wilson (2010), Evolution of Neogene volcanism and stress patterns in the glaciated West Antarctica Rift, Marie Byrd Land, Antarctica, *J. Geol. Soc. London*, *167*, 401–416, doi:10.1144/0016-76492009-044.
Petrunin, A. G., I. Rogozhina, A. P. M. Vaughan, I. T. Kukkonen, M. K. Kaban, I. Koulakov, and M. Thomas (2013), Heat flux variations beneath central Greenland's ice due to anomalously thin lithosphere, *Nat. Geosci.*, *6*, 746–750, doi:10.1038/ngeo1898.
Phipps Morgan, J., and B. K. Holtzman (2005), Vug waves: A mechanism for coupled rock deformation and fluid migration, *Geochem. Geophys. Geosyst.*, *6*, Q08002, doi:10.1029/2004FC000818.
Pollack, H. N., S. J. Hurter, and J. R. Johnson (1993), Heat flow from the Earth's interior: Analysis of the global data set, *Rev. Geophys.*, *31*, 267–280, doi:10.1029/93RG01249.
Pollard, D., R. M. DeConto, and A. A. Nyblade (2005), Sensitivity of Cenozoic Antarctic ice sheet variations to geothermal heat flux, *Global Planet. Change*, *49*, 63–74, doi:10.1016/j.gloplacha.2005.05.003.
Pourpoint, M., S. Anandakrishnan, C. J. Ammon, and C. Chai (2015), Crustal and upper mantle velocity structure of Greenland from ambient noise and earthquake surface wave tomography, AGU Fall Meeting, S23D-2783, San Francisco, Calif.
Rickers, F., A. Fichtner, and J. Trampert (2013), The Iceland-Jan Mayen plume system and its impact on mantle dynamics in the North Atlantic region: Evidence from full-waveform inversion, *Earth Planet. Sci. Lett.*, *367*, 39–51, doi:10.1016/j.epsl.2013.02.022.
Ritz, C., and Grenoble team members (1997), Intercomparison experiment: Comparison of existing Greenland models, doi:10.1.1.604.2412.
Rogozhina, I., J. M. Hagedoorn, Z. Martinec, K. Fleming, O. Soucek, R. Greve, and M. Thomas (2012), Effects of uncertainties in the geothermal heat flux distribution on the Greenland Ice Sheet: An assessment of existing heat flow models, *J. Geophys. Res.*, *117*, F02025, 1–16, doi:10.1029/2011JF002098.
Rogozhina, I., A. G. Petrunin, A. P. M. Vaughan, B. Steinberger, J. V. Johnson, M. K. Kaban, R. Calov, F. Rickers, M. Thomas, and I. Koulakov (2016), Melting at the base of the Greenland ice sheet explained by Iceland hotspot history, *Nat. Geosci.*, *9*, 366–369, doi:10.1038/NGEO2689.
Rubin, A. M. (1995a), Getting granite dikes out of the source region, *J. Geophys. Res.*, *100*, 5911–5929, doi:10.1029/94JB02942.
Rubin, A. M. (1995b), Propagation of magma-filled cracks, *Annu. Rev. Earth Planet. Sci.*, *23*, 287–336, doi:10.1146/annurev.ea.23.050195.001443.
Schroeder, D. M., D. D. Blankenship, D. A. Young, and E. Quartini (2014), Evidence for elevated and spatially variable geothermal flux beneath the West Antarctic Ice Sheet, *Proc. Natl. Acad. Sci. U.S.A.*, *111*(25), 9070–9072, doi:10.1073/pnas.140518411.
Shackleton, N. J., et al. (1984), Oxygen isotope calibration of the onset of ice-rafting and history of glaciation in the North Atlantic region, *Nature*, *307*, 620–623, doi:10.1038/307620a0.
Shapiro, N. M., and M. H. Ritzwoller (2004), Inferring surface heat flux distributions guided by a global seismics model: Particular application to Antarctica, *Earth Planet. Sci. Lett.*, *223*, 213–224, doi:10.1016/j.epsl.2004.04.011.
Sigvaldason, G. E., K. Annertz, and M. Nilsson (1992), Effect of glacier loading/deloading on volcanism: Postglacial volcanic production rate of the Dyngjufjöll area, central Iceland, *Volcanology*, *54*, 385–392, doi:10.1007/bf00312320.
Stern, T. A., and U. S. Ten Brink (1989), Flexural uplift of the Transantarctic Mountains, *J. Geophys. Res.*, *94*, 10,315–10,330, doi:10.1029/JB094iB08p10315.
Sternai, P., L. Caricchi, S. Castelltort, and J.-D. Champagnac (2016), Deglacial and glacial erosion: A joint control on magma productivity by continental unloading, *Geophys. Res. Lett.*, *43*, 1632–1641, doi:10.1002/2015GL067285.
Stewart, I. S., J. Sauber, and J. Rose (2000), Glacio-seismotectonics: Ice sheets, crustal deformation and seismicity, *Quat. Sci. Rev.*, *19*, 1367–1389, doi:10.1016/S0277-3791(00)00094-9.
Timoshenko, S. P., and K. Woinowsky-Krieger (1959), *Theory of Plates and Shells*, McGraw-Hill, New York.
Turcotte, D. L., and G. Schubert (1982), *Geodynamics*, 3rd ed., Cambridge Univ. Press, Cambridge, U. K.

van den Berg, J., R. S. W. van de Wal, G. A. Milne, and J. Oerlemans (2008), Effect of isostasy on dynamical ice sheet modeling: A case study for Eurasia, *J. Geophys. Res.*, *113*, B05412, doi:10.1029/2007JB004994.

Watts, A. B. (2001), *Isostasy and Flexure of the Lithosphere*, Cambridge Univ. Press, Cambridge, U. K.

Wolf, D. (1987), An upper bound on lithosphere thickness from glacio-isostatic adjustment in Fennoscandia, *J. Geophys.*, *61*, 141–149.

Wu, P., and H. S. Hasegawa (1996), Induced stresses and fault potential in eastern Canada due to a realistic load: A preliminary analysis, *Geophys. J. Int.*, *127*, 215–229, doi:10.1111/j.1365-246X.1996.tb00008.x.

Zielinski, G. A., P. A. Mayewsky, L. D. Meeker, S. Whitlow, M. S. Twickler, M. Morrison, D. A. Meese, A. J. Gow, and R. B. Alley (1994), Record of volcanism since 7000 B.C. from the GISP2 Greenland ice core and implications for the volcano-climate system, *Science*, *264*, 948–952, doi:10.1126/science.264.5161.948.

Zielinski, G. A., P. A. Mayewsky, L. D. Meeker, S. Whitlow, and M. S. Twickler (1996), A 110,000-yr record of explosive volcanism from the GISP2 (Greenland) ice core, *Quat. Res.*, *45*(2), 109–118, doi:10.1006/qres.1996.0013.